

level version of our computer code which should permit more meaningful data analysis.

- Auer, L. H., Rees, D. E., and Stenflo, J. O., *Astron. Astrophys.*, **88**, 302 (1980).
 Cram, L. E., *Proc. Astron. Soc. Aust.*, **5**, (1983).
 Gingerich, O., Noyes, R. W., and Kalkofen, W., *Solar Phys.*, **18**, 347 (1971).
 Rees, D. E., and Saliba, G. J., *Astron. Astrophys.*, **115**, 1 (1982).
 Stenflo, J. O., *Astron. Astrophys.*, **84**, 68 (1980).
 Vernazza, J. E., Avrett, E. H., and Loeser, R., *Astrophys. J. Suppl. Ser.*, **45**, 635 (1981).

Electron Cyclotron Masers during Solar Flares

S. M. White and D. B. Melrose, *Dept. of Theoretical Physics, Uni. of Sydney*, and G. A. Dulk*, *CSIRO Division of Radiophysics*

1. Introduction

It has been suggested (Holman *et al* 1980; Melrose and Dulk 1982a) that solar microwave spike bursts are due to electron cyclotron maser action. These bursts have been observed in the range 1-3 Ghz, and occur in conjunction with flare-associated impulsive microwave and hard X-ray bursts. The bursts have rise times of a millisecond or less (e.g. Slottje 1978). Their high brightness temperatures, exceeding 10^{12} K, and high degrees of circular polarization ($\approx 100\%$) favour a coherent emission mechanism such as cyclotron maser emission. Melrose and Dulk (1982b) suggested that a large fraction of the energy in the flare can be radiated through cyclotron maser emission as the fundamental. Such radiation does not escape the Sun, but is reabsorbed at the second harmonic of the cyclotron frequency. This leads to radiofrequency heating of regions around, but removed from, the flare site. In order to investigate the radiofrequency heating it is important to determine how the maser emission turns on and where it originates in relation to the flare itself. It is our purpose in this paper to explore a simple model for the dynamics of the electrons which produce the maser emission and to use the model to investigate the conditions under which the maser turns on. In section 2 we discuss the magnetic field in the flaring region in terms of a parabolic model, and solve for the motion of a particle in this model. In section 3 we discuss the two simple limiting cases of impulsive and continuous injection of energetic particles, and discuss the evolution of the distribution functions in each case. In section 4 we describe the theory of cyclotron maser action and show how it applies to the models, and in section 5 we discuss the implications of our results.

*on leave from Dept. of Astro-Geophysics, University of Colorado, Boulder.

2. Particle Dynamics in a Magnetic Flux Tube

We assume that the particles responsible for the microwave spike bursts are energetic electrons in a coronal magnetic flux tube shaped like an arch, its two footpoints embedded in the dense solar atmosphere. It is commonly thought that solar flares occur when twisted field lines in such arches suddenly reconnect and relax, releasing large amounts of energy. Some of this energy heats the ambient plasma, producing the required energetic electrons. We assume that the magnetic field is minimum at the top of the arch and increasing towards the footpoints. We suppose that the creation of energetic particles occurs at the top of the arch, although the model may easily be changed to accommodate another release site. The electrons travel down the flux tube and either mirror at a certain height above the atmosphere, or precipitate into the dense chromospheric plasma and thermalize, producing the observed hard X-ray bursts.

Let s denote the distance along a field line from the top of the arch; s is positive for one leg and negative for the other. We suppose that the magnetic field varies with distance along a field line according to a parabolic law

$$B(s) = B_0(1+s^2/d^2) \quad (1)$$

where d is a scale length for changes in the magnetic field and B_0 is the field at the top of the arch. A recent study showed two examples of $H\alpha$ loops in active regions which were well-fitted by a dipole model (Chen Chuan-Le and Loughhead 1983) and (1) is a reasonable approximation to this. We ignore the curvature of the loop, assuming its effects to be negligible as long as the radius of curvature is much larger than the gyro radius. Any twisting of the field lines is seen by the particles as merely increasing the distance over which the field changes, i.e., an increase in d .

Neglecting scattering, the motion of particles in the flux tube is described by

$$m \frac{d\mathbf{v}}{dt} = q\mathbf{v} \times \mathbf{B} \quad (2)$$

which reduces with the above assumptions (e.g. see Northrop, 1963) to

$$|v| = \text{constant}, \quad (3)$$

$$\sin^2 \alpha_B(s) = \text{constant}, \quad (4)$$

and

$$\frac{d^2 s}{dt^2} = -v^2 \sin^2 \alpha_0 / 2\Omega_0 \cdot \frac{d\Omega}{ds}(s) \quad (5)$$

where α is the pitch angle of the particle, i.e. the angle between \mathbf{B} and the velocity \mathbf{v} , $\Omega(s) = qB(s)/mc$ is the gyrofrequency, and a subscript zero denotes the value of the quantity at $s=0$. When we solve (5) with the magnetic field (1), to find

$$s(t) = d \cdot \cot \alpha_0 \sin\{v(t-t_0) \sin \alpha_0 / d\}. \quad (6)$$

The time t_0 may be interpreted as the first time (after injection at $t=0$) that the particle crosses the point $s=0$. Rather than label an orbit with t_0 we may use instead the position of the particle at $t=0$, s_0 . In the next section we need to express s_0

in terms of the local quantities s , t and α . On inverting (6) we find that the relation is

$$s_0 = s \cdot \cos\left\{\frac{vt \cdot \sin\alpha}{\sqrt{(d^2+s^2)}}\right\} - \sqrt{(d^2+s^2)} \cot\alpha \cdot \sin\left\{\frac{vt \cdot \sin\alpha}{\sqrt{(d^2+s^2)}}\right\}. \quad (7)$$

The pitch angle α at a height s is related to its value at $s = 0$, α_0 , by (4), namely

$$\cos^2\alpha_0 = (d^2 \cos^2\alpha + s^2) / (d^2 + s^2). \quad (8)$$

From (6), we see that the particle's motion is periodic. The bounce period is

$$T = 2\pi d / (v \cdot \sin\alpha_0). \quad (9)$$

It reaches a maximum depth in the flux tube of $d \cdot \cot\alpha_0$ before it mirrors and returns up the flux tube. Thus the period depends only on the velocity of the particle perpendicular to the field at $s = 0$, and its penetration depends only on its pitch angle there.

Suppose that the dense solar atmosphere lies at $|s| \geq h$. Then particles for which

$$d \cdot |\cot\alpha_0| > h \quad (10)$$

strike the atmosphere and lose their energy by collisions. They are unable to return up the flux tube, leaving a depletion of upgoing particles. At a height $0 < s < h$ the pitch angle range

$$\cos\alpha < -\sqrt{(h^2 - s^2) / (h^2 + d^2)} \quad (11)$$

is empty, implying a loss cone anisotropy. In practice, the boundary of the solar atmosphere is not sharp and there is a range of pitch angles over which the distribution drops to zero in the loss cone. Loss cones have been exhaustively discussed elsewhere, and a distribution with a loss cone is known to be unstable to electron cyclotron maser action (Wu and Lee 1979; Hewitt, Melrose and Rönmark 1982).

In the next section we use these results for a single particle to study how a distribution evolves.

3. Models for Energetic Particle Injection

The nature of the evolution of the distribution function depends on the time scales involved in the injection of energetic particles (i.e. heating of the ambient plasma). We discuss two limiting cases. In the first we assume that the injection process is much shorter than typical dynamical time scales for particle motion, so that essentially no particles leave the heated region before the heating ceases. We model the source as an instantaneously heated region around $s = 0$. This is the impulsive model. In the second we assume that heating takes place on a time scale longer than dynamical time scales such as (9), and model the injection by a continuous, constant source of particles at $s = 0$.

To determine the evolution of the distribution in each case we must solve Boltzmann's equation

$$\frac{\partial f}{\partial t} + \mathbf{v} \cdot \frac{\partial f}{\partial \mathbf{r}} + \frac{d\mathbf{p}}{dt} \cdot \frac{\partial f}{\partial \mathbf{p}} = S(\mathbf{r}, \mathbf{p}, t) \quad (12)$$

where the right hand side of (12) is the source term appropriate to the model. We use the method of characteristics to solve (12), drawing on the orbit solutions found in the last section.

For the impulsive model the source term is

$$S(\mathbf{r}, \mathbf{p}, t) = n \cdot \delta(t) \cdot f_0(v, \cos\alpha) \cdot G(s_0) \quad (13)$$

where n is a particle density in the heated region and $\delta(t)$ denotes a Dirac delta function in time. f_0 is the velocity distribution at $t = 0$, and $G(s_0)$ is a distribution describing the spatial extent of the heated region. For example, in figures shown in this paper we choose

$$G(s_0) = \exp(-s_0^2 / 2l^2) \quad (14)$$

where l is the scale length of the heated region. In using the form (13) we are assuming that $l \ll d$, so that a particle's pitch angle does not change in traversing the heated region.

When we solve (12) with the source term (13), we find the solution

$$f(\mathbf{r}, \mathbf{p}, t) = n \cdot f_0\left(v, \left\{\frac{d^2 \cos^2\alpha + s^2}{\sqrt{(d^2 + s^2)}}\right\}^{1/2}\right) \cdot G\left(s \cdot \cos\left\{\frac{vt \sin\alpha}{\sqrt{(d^2 + s^2)}}\right\}\right) - \sqrt{(d^2 + s^2)} \cdot \cot\alpha \cdot \sin\left\{\frac{vt \sin\alpha}{\sqrt{(d^2 + s^2)}}\right\}. \quad (15)$$

We must impose on this the loss cone feature (11), which is not relevant until times greater than about a bounce period. In addition, there is a background thermal distribution which is not important for the discussion here.

Example of the distribution (15) are shown in Figure 1 (at a time much less than a bounce period) and Figure 2 (after several bounce periods). Downgoing particles lie in the right-hand quadrant and upgoing particles in the left-hand quadrant. The basic form of the distribution may be seen by considering the case $l = 0$, i.e. when initially there are particles present only at $s = 0$. Then equation (7) implies

$$x = y \cdot \cot\alpha \quad (16)$$

with

$$x = v_{\parallel} t / s \quad (17)$$

and

$$y = v_{\perp} t / \sqrt{(d^2 + s^2)} \quad (18)$$

and where $v_{\parallel} = v \cdot \cos\alpha$ and $v_{\perp} = v \cdot \sin\alpha$ are the velocities parallel and perpendicular to the field respectively. By convention, velocity distributions are shown as contour plots with v_{\parallel} and v_{\perp} as axes. In this case the plot is just a single line described by (16), since at a point s at a time t only a one-parameter family of particles are present. Allowing a spread in s_0 leads to a spread in velocity space, as in Figure 1, with this spread dependent on the assumed form of $G(s_0)$.

For the continuous model we use the source term

$$S(\mathbf{r}, \mathbf{p}, t) = R \cdot \delta(s) \cdot f_0(v, \cos\alpha) \quad (19)$$

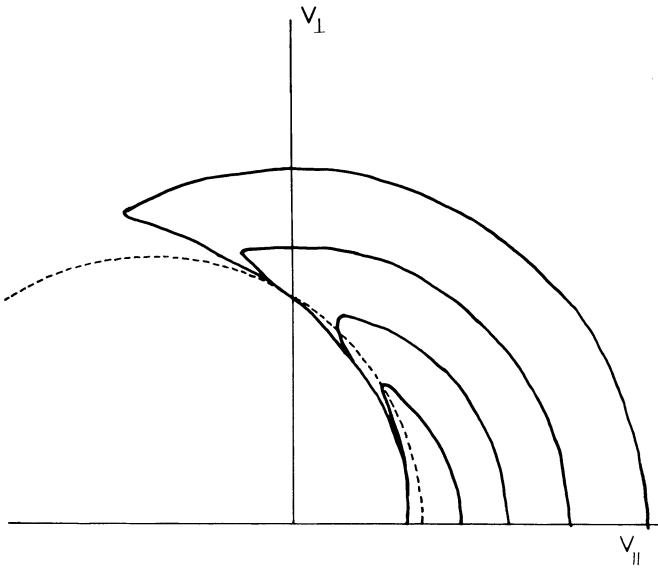


Figure 1. A contour plot of the distribution in the impulsive model. The initial velocity distribution is taken to be $f_0(v, \cos \alpha) \propto (v/v_T)^{-6}$, where v_T is a characteristic thermal speed. Other parameters for this plot are $s/d=2$, $tv_T/d=2$, $l/d=0.5$ and $h/d=4$, where s is the height in the flux tube, t is the time, d is the scale length of the magnetic field, l is the scale length of the impulsively heated region and h is the depth at which the dense chromosphere is encountered. The dashed semicircle is an integration contour for the maser growth rate (see section 4). The contour levels are logarithmically spaced.

where R is an injection rate in particles per unit area (at $s=0$) per unit time. The source is idealized as infinitesimally small and constant in time. The solution of (12) with the source (19)

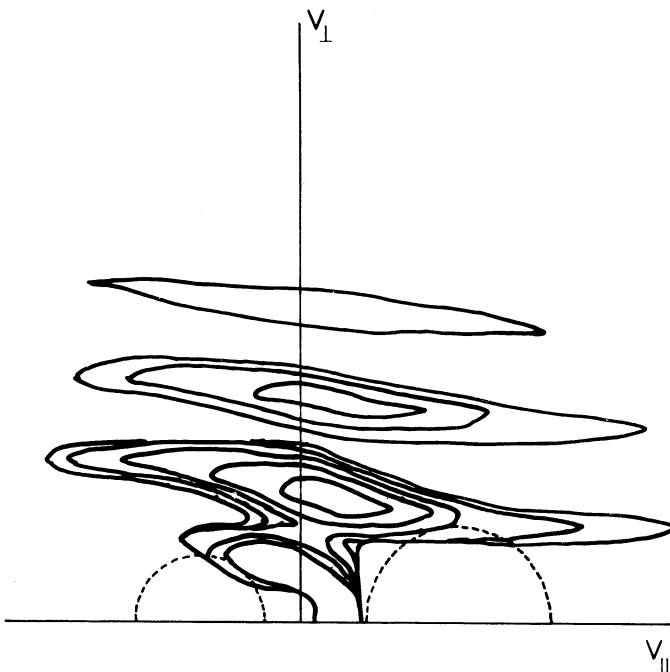


Figure 2. A contour plot of the impulsive model at $t=12$, all other parameters being as in Figure 1.

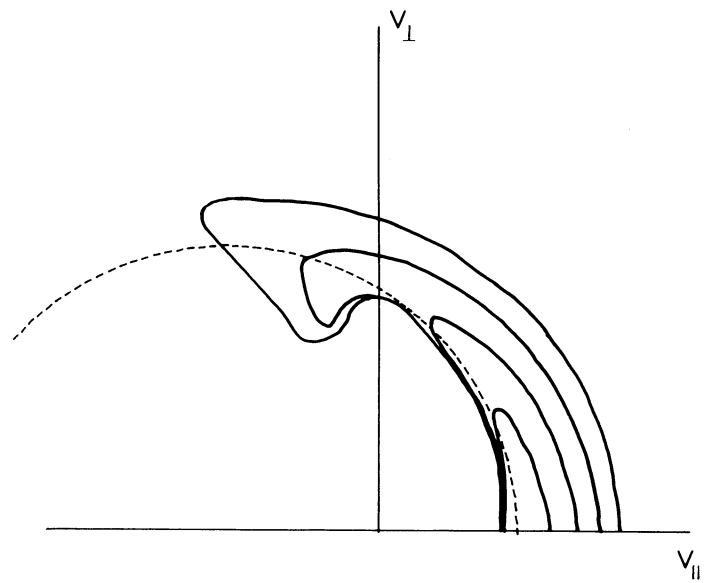


Figure 3. A contour plot for the continuous model, with $s=2$, $t=2$ and $h=4$.

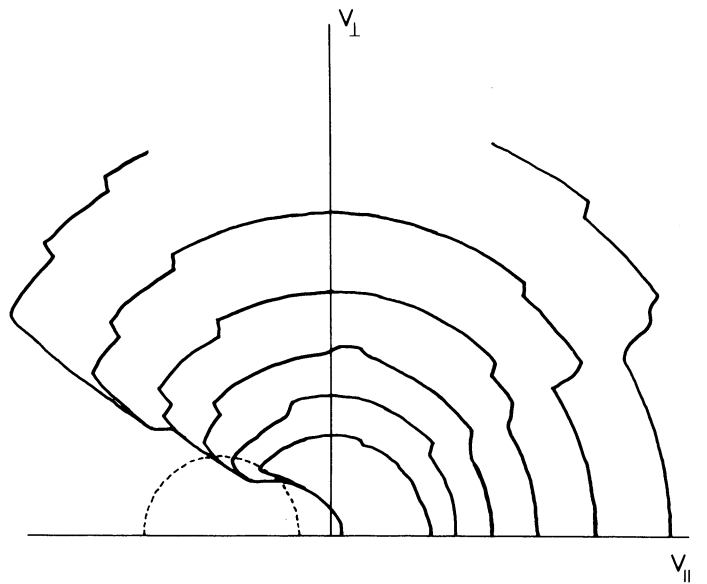


Figure 4. A contour plot for the continuous model at a later time, $t=12$.

is zero in a given velocity range at fixed s and t until the appropriate particles have had enough time to reach that depth, and thereafter the distribution is

$$f(r, p, t) = R \cdot f_0 \left(v, \left\{ \frac{d^2 \cos^2 \alpha + s^2}{d^2 + s^2} \right\}^{1/2} \right) \cdot \frac{1 + \text{int} \{ v(t - t_0) \sin \alpha / \pi / \sqrt{d^2 + s^2} \}}{v \left\{ \frac{d^2 \cos^2 \alpha + s^2}{d^2 + s^2} \right\}^{1/2}} \quad (20)$$

where $\text{int}(x)$ denotes the integer part of the number x . The presence of this function represents an idealization due to the assumption that the assumed source has an abrupt edge and turns on instantaneously. At early times the argument of the integer function is less than and the distribution is similar to that for the impulsive model (Figure 3). The left-hand edge of the distribution looks like the line described by equation (16), but to the right (larger v_{\parallel}) the distribution is filled in according to the initial distribution f_0 . At later times the dominant features of the distribution are the downgoing (due to the presence of the atmosphere in the opposite leg) and upgoing loss cones (Figure 4). As we show in the next section the loss cones allow maser action to occur.

4. Electron Cyclotron Masers

The theory of electron cyclotron masers has recently been reevaluated and shown to imply higher growth rates under milder conditions than previously thought (Wu and Lee 1979; Hewitt *et al* 1982). Rather than discuss the theory in detail, we mention here only the features needed to investigate the distributions of the preceding section. A single electron is in cyclotron resonance with a wave of frequency ω and wavevector \mathbf{k} at the p -th harmonic if it satisfies the condition

$$\omega - k_{\parallel} v_{\parallel} - p\Omega/\gamma = 0, \quad (21)$$

where k_{\parallel} is the component of the wavevector parallel to the magnetic field, Ω is the local gyrofrequency and $\gamma = (1 - v^2/c^2)^{-1/2}$. The growth rate for a given distribution involves an integral over the contributions of all resonant particles. On the $v_{\perp} - v_{\parallel}$ diagram these particles lie on a half-ellipse given by the solution of (21). Under semirelativistic conditions ($k_{\parallel}c/p\omega \ll 1$) the ellipse becomes a semicircle

$$(v_{\parallel} - v_0)^2 + v_{\perp}^2 = V^2 \quad (22)$$

where v_0 and V are functions of the wave parameters ω and k_{\parallel} (Hewitt *et al* 1982). Thus different circles correspond to different waves. In this limit, the growth rate for a particular wave is just an integral around the appropriate half-circle,

$$\Gamma(p, \omega, \mathbf{k}) = A(p, \omega, \mathbf{k}) \int_0^{\pi} d\phi v_{\perp}^{2p} \frac{\partial f}{\partial v_{\perp}} \quad (23)$$

where A is a function of the wave parameters, $v_{\parallel} = v_0 - V \cos \phi$ and $v_{\perp} = V \sin \phi$. According to (23), growth occurs for any wave whose semicircle lies mostly in regions where $\partial f / \partial v_{\perp} > 0$. If such a circle can be drawn then maser action should take place.

On each of the four figures we have drawn circles whose intersections with the distributions occur in regions in which $\partial f / \partial v_{\perp} > 0$. Thus waves corresponding to these circles should grow. It should be apparent from the general properties of the solutions (in particular, from the shape of (16)) that it is always possible to find such circles at early times, in both of our models. Thus we expect that electron cyclotron maser action should be a common feature during solar flares.

5. Discussion

We have shown that there are two phases in which maser action is likely to occur following a solar flare. In the later

phase, loss cones in upgoing particles develop and are unstable to wave growth, as has been assumed by Holman *et al* (1980) and Melrose and Dulk (1982a). The resulting maser produces radiation at low harmonics.

It is pointed out for the first time here that maser action is also likely to occur in an earlier phase when the particles are predominantly downgoing (e.g. see Figure 1). The resulting maser emits radiation which should be reflected or reabsorbed at a level where its frequency equals the critical frequency for the appropriate mode. The radiation propagates nearly perpendicular to the field lines so heating over a large area is possible. Growth rates in the earlier phase are expected to be high, but so far no detailed calculations for growth rate have been performed for this case.

Once the maser turns on, the distributions are modified through scattering by the radiation. After a number of growth times radiation should reach a level at which significant pitch angle scattering occurs, reducing the value of $\partial f / \partial v_{\perp}$ and tending to switch the maser off. This self-quenching effect of a cyclotron maser corresponds to saturation in a laboratory maser (Melrose and Dulk 1982a).

In conclusion, this study has shown that it is not sufficient to study only masers due to loss cone anisotropies in upgoing particles when investigating radiofrequency heating in flares. Maser emission seems likely to occur in an earlier downgoing phase. The implications of this result have yet to be adequately understood.

References

- Chen Chuan-Le, and R. E. Loughhead, *Proc. Astron. Soc. Aust.*, **5**, (1983).
 Hewitt, R. G., D. B. Melrose, and K. G. Rönmark, *Aust. J. Phys.*, **35**, 447 (1982).
 Holman, G. D., D. Eichler, and M. R. Kundu, in *IAU Symposium 86, Radio Physics of the Sun*, ed. M. Kundu and T. Gergely (Dordrecht: Reidel), p. 205 (1980).
 Melrose, D. B., and G. A. Dulk, *Astrophys. J.*, **259**, 844 (1982a).
 Melrose, D. B., and G. A. Dulk, *Astrophys. J. Lett.*, **259**, L41 (1982b).
 Northrop, T. G., *The Adiabatic Motion of Charged Particles* (Wiley: New York), p. 9 (1963).
 Slottje, C., *Nature*, **275**, 520 (1978).
 Wu, C. S., and L. C. Lee, *Astrophys. J.*, **230**, 621 (1979).

Drifting Subpulses in Pulsars

Michelle C. Allen and D. B. Melrose, *School of Physics, University of Sydney*

1. Introduction

Individual pulses from a given pulsar can differ greatly in both shape and intensity, and are often made up of narrower 'subpulses', i.e. local emission peaks one tenth the width of the mean pulse. Properties such as shape, polarization and